Japanese Journal of Applied Physics
Vol. 47, No. 8, 2008, pp. 6448–6451

Thickness Dependences of Polarization Characteristics in Mn-Substituted $BiFeO_3$ Films on Pt Electrodes

Zhiyong ZHONG*, Yoshihiro SUGIYAMA[1], and Hiroshi ISHIWARA

Interdisciplinary Graduate School of Science and Engineering, Tokyo Institute of Technology, 4259 Nagatsuta, Midori-ku, Yokohama 226-8503, Japan
[1]*Fujitsu Laboratories, Ltd., 10-1 Morinosato-Wakamiya, Atsugi, Kanagawa 243-0197, Japan*

(Received February 20, 2008; accepted April 25, 2008; published online August 8, 2008)

The thickness dependences of polarization characteristics have been measured for Mn-substituted $BiFeO_3$ (BFO) films formed on $Pt/Ti/SiO_2/Si(100)$ substrates by chemical solution deposition (CSD). X-ray diffraction (XRD) patterns have proved the existence of a dielectric phase, which is mainly formed at the initial stage of the film formation. It has been revealed that the remanent polarization (P_r) increases and the coercive electric field (E_c) decreases with increasing film thickness. It has also been found from the thickness-dependent polarization characteristics that the equivalent oxide thickness (EOT) of the dielectric layers at the interfaces and the intrinsic coercive field in the ferroelectric layers are 4.5 nm and approximately 90 kV/cm, respectively, in both 3 and 5% Mn-substituted BFO films. [DOI: 10.1143/JJAP.47.6448]

KEYWORDS: $BiFeO_3$, intrinsic coercive field, passive layer, remanent polarization, ferroelectric

1. Introduction

Ferroelectric random access memories (FeRAMs) have been attracting much attention because of their nonvolatility, low power consumption, and high operation speed. The current mass production of FeRAMs is subject to a limitation of storage capability because the remanent polarization (P_r) in current ferroelectric materials such as $PbZr_xTi_{1-x}O_3$ (PZT) and $SrBi_2Ta_2O_9$ (SBT) is not necessarily large. One of the candidate ferroelectrics in future high-density FeRAMs with small ferroelectric capacitor sizes is $BiFeO_3$ (BFO), which has a P_r value of as large as 90 μC/cm^2.[1)] BFO is also important as a multiferroic material, which exhibits ferroelectricity, ferromagnetism, and ferroelasticity simultaneously.

Wang *et al.* investigated epitaxial BFO thin films deposited on $SrTiO_3$ substrates and obtained excellent ferroelectricity at room temperauture (RT).[1)] We have been studying polycrystalline BFO thin films formed on Pt,[2)] Ir,[3)] and $SrRuO_3$[4)] electrodes, focusing on applications to high-density FeRAMs. We have succeeded in suppressing the leakage current density in BFO thin films, while maintaining a high value of P_r by partially substituting Mn atoms for Fe atoms.[2)] However, the polarization reversal voltage in BFO capacitors is still high, and thus a decrease of the operation voltage is essential to enable the use of BFO films in future FeRAMs.

It is known that in a ferroelectric capacitor, a thin dielectric layer with a low dielectric constant often exists between the ferroelectric film and the electrode. It is called a passive layer, or a dead layer, and is nonswitchable upon the application of bipolar voltage pulses. The first study on passive layers was carried out by Merz more than 50 years ago.[5)] More recently, Tagantsev and Gerra[6)] theoretically predicted many characteristics of PZT, which have been confirmed by experimental data. In this paper, we measure the film thickness dependences of polarization characteristics in Mn-substituted BFO films and derive both the EOT value of the passive layer and the intrinsic coercive electric field in the ferroelectric layers, using Tagantsev and Gerra's formula.

*E-mail address: zhong.z.aa@m.titech.ac.jp

2. Sample Preparation

Stoichiometric 3 and 5% Mn-substituted BFO solutions of 0.33 mol/kg (Toshima) were spin-coated at 3000 rpm for 30 s on $Pt/Ti/SiO_2/Si(100)$ substrates. They were then baked on a hot plate at 240 °C for 3 min, and calcined at 350 °C for 10 min in air. After this process, a BFO film of 20–30 nm thickness was formed. This process was repeated approximately 2 to 40 times to obtain films of designated thicknesse; the thicknesses for both 3 and 5% Mn-substituted BFO films were designated to be 50, 100, 200, 400, 600, and 800 nm. Finally, the deposited films were annealed at 600 °C for 10 min in nitrogen.

Next, Pt top electrodes of 3.14×10^{-2} and 0.79×10^{-2} mm^2 in area were deposited at RT by electron-beam evaporation through a shadow mask. The pressure during deposition was typically 5×10^{-6} Torr. The crystal structures of the films were determined by a multipurpose X-ray diffractometer (XRD). The electrical properties of MFM (M: metal, F: ferroelectric) capacitors were measured by a ferroelectric test system (Toyo FCE_fast) and a precision semiconductor parameter analyzer (HP 4156C).

3. Experimental Results

The thicknesses of the BFO films were measured by an α-stepper. The actual values were somewhat different from the designated ones; they were 60, 120, 240, 480, 720, and 960 nm for the 3% Mn-substituted films and 55, 110, 220, 440, 660, and 880 nm for the 5% Mn-substituted films. In the films thicker than 500 nm, a number of microcracks were observed by an optical microscope. By contrast, a good surface without any cracks was observed in the films thinner than 500 nm. The microcracks may be generated by the shrinkage of the films during the crystallization annealing or by the mismatch of the thermal expansion coefficients during cooling.

Figure 1 shows XRD patterns of 5% Mn-substituted BFO films with various thicknesses. Each peak is indexed by a rhombohedral structure of $BiFeO_3$. The figure shows that the peak intensity regularly increases with increasing film thickness and that a secondary phase of $Bi_2Fe_4O_9$ is seen only in the thinnest film, in which the contribution of

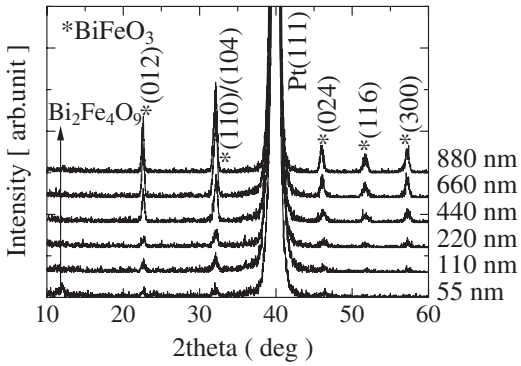

Fig. 1. XRD patterns of 5% Mn-substituted BFO films with different thicknesses.

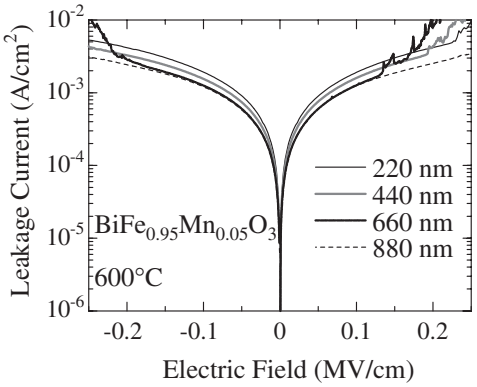

Fig. 2. *J–E* characteristics of 5% Mn-substituted BFO films with different thicknesses.

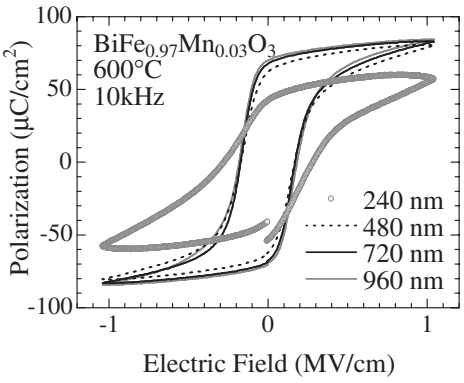

(a)

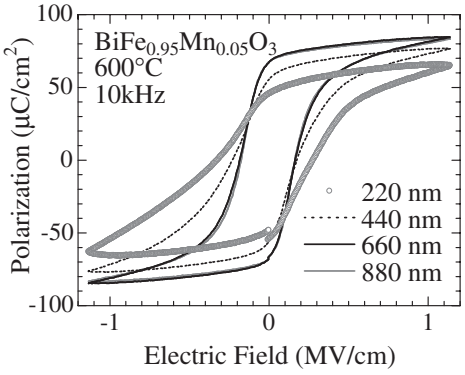

(b)

Fig. 3. Hysteresis loops of 3% (a) and 5% (b) Mn-substituted BFO films with different thicknesses measured at 10 kHz.

a dielectric passive layer might be large relative to the ferroelectric layer. A $Bi_2Fe_4O_9$ phase has also been observed in our previous samples formed under the same conditions.[7] Similar XRD patterns were obtained for 3% Mn-substituted films, but the peak intensity corresponding to the $Bi_2Fe_4O_9$ phase was weaker. The existence of the dielectric passive layer is further confirmed from the polarization characteristics of the BFO capacitors.

The leakage current characteristics of the Mn-substituted BFO films were investigated. The films with 55 and 60 nm thicknesses broke down as soon as a low voltage was applied. The leakage current densities in the 110- and 120-nm-thick films were also very high. These results imply that serious leakage paths exist in the thin Mn-substituted BFO films. Figure 2 shows the current density vs electric field (*J–E*) characteristics of 5% Mn-substituted BFO films thicker than 220 nm. The figure shows that the leakage current density ranges on the order of 10^{-3} A/cm^2 and that the breakdown field is reduced for the thinner films. The same tendency of leakage current density was obtained in 3% Mn-substituted films.

Figures 3(a) and 3(b) show the polarization vs electric field (*P–E*) characteristics of 3 and 5% Mn-substituted BFO films, respectively. The measurement frequency was 10 kHz. It was difficult to measure the polarization characteristics accurately in the capacitors with 110- and 120-nm-thick BFO films because of the high leakage currents. As shown in the figures, the remanent polarization (P_r) increases and the coercive electric field (E_c) decreases with increasing film thickness. The values of P_r and E_c in the 880-nm-thick 5% Mn-substituted BFO film were 68 μC/cm^2 and 170 kV/cm at an applied electric field of 1.1 MV/cm, respectively. We conclude from these electrical measurements that the microcracks observed in the films thicker than 500 nm do not significantly affect the insulating and ferroelectric characteristics.

4. Discussion

The thickness-dependent polarization characteristics shown in Fig. 3 are assumed to originate from the existence of a dielectric layer in the vicinity of the bottom electrode. Actually, the existence of the $Bi_2Fe_4O_9$ phase has been observed by XRD analysis, as shown in Fig. 1. The physical model and the equivalent circuit of the capacitors are shown in Fig. 4, where h and d are the thicknesses of the ferroelectric and dielectric layers, respectively, and ε_f and ε_d are their dielectric constants. In the equivalent circuit, the external voltage V is divided into V_f and V_d, where V_f and V_d are voltages applied to the ferroelectric and dielectric layers, respectively, and C_f and C_d are their capacitances.

First, we consider a simple model where no current flows across the both ferroelectric and dielectric capacitors, and thus the charge neutrality condition is satisfied at the node between the two capacitors. In this model, the apparent *P–V* characteristics can be derived graphically from the original *P–V*$_f$ characteristics of the ferroelectric layer, using the relations of $V = V_f + V_i$ and $Q = C_i V_i$ (Q: induced electric charge), and the fact that P is approximately equal to the

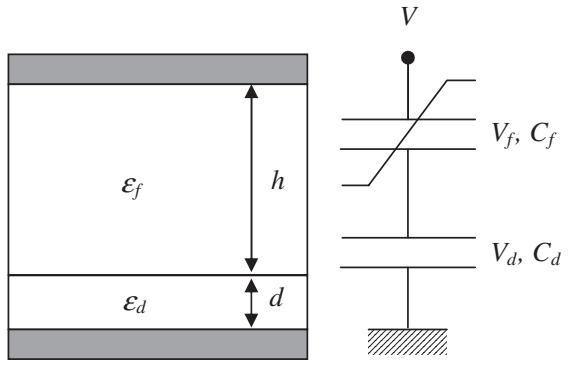

Fig. 4. Ferroelectric capacitor model composed of dielectric and ferroelectric layers and its equivalent circuit.

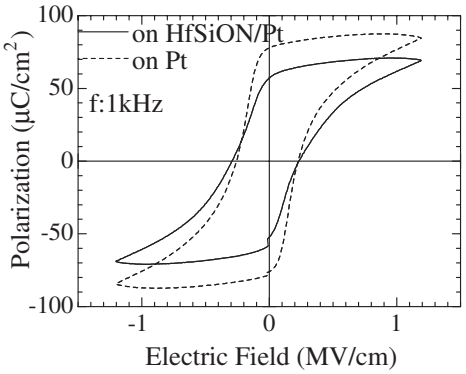

Fig. 5. Comparison of hysteresis loops between Pt/BFO/Pt and Pt/BFO/HfSiON/Pt capacitor structures measured at 1 kHz.

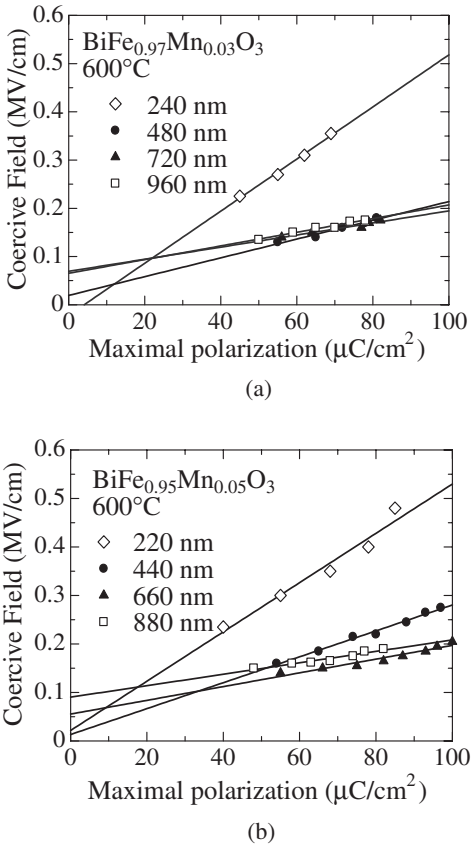

Fig. 6. Relationships between P_m and E_c in capacitors containing 3% (a) and 5% (b) Mn-substituted BFO films with different thicknesses. Data along each line were obtained by varying the applied electric field.

induced charge density in a high-dielectric-constant material. The obtained P–V characteristics are stretched in the horizontal direction, while maintaining the two intercepts ($-V_c$ and V_c) with the horizontal axis. That is to say, the important features in the P–V characteristics are that the remanent polarization decreases but the coercive voltage does not change with the existence of a dielectric layer. This result also shows that the apparent coercive field does not change when the dielectric layer is thin.

The validity of this simple model was experimentally ascertained by inserting a 4-nm-thick dielectric HfSiON layer between an 840-nm-thick BFO film and a Pt bottom electrode. Typical P–E characteristics measured at 1 kHz are shown in Fig. 5, in which P_r decreases significantly in the dielectric-layer-inserted capacitor, but the increase in E_c is slight. From the P–E characteristics in Fig. 3, it is clear that a more sophisticated model is needed to explain the pronounced increase in the coercive electric field.

It is known that trapped charges in the vicinity of the electrodes are crucial for changing the E_c value in P–E characteristics.[8–10] When charges are injected by a high electric field to the dielectric/ferroelectric interfaces in a ferroelectric capacitor with dielectric passive layers, some of them might remain there even after the electric field is reduced to E_c. Thus, a larger electric field is necessary to repel these charges, and the apparent value of E_c increases.

Tagantsev and Stolichnov proposed useful equations to describe the behavior of a ferroelectric capacitor, in which charge injection through the passive layer is not neglected.[11] The physical structure of the capacitor is the same as that shown in Fig. 4. The equations are given in eqs. (1) and (2) as follows, assuming that $d \ll h$:

$$E_c = \begin{cases} E_{c0} + \dfrac{d}{h} \times \dfrac{1}{\varepsilon_0 \varepsilon_d}(P_m - \varepsilon_0 \varepsilon_d E_{th}) & \\ \qquad\qquad (\varepsilon_0 \varepsilon_d E_{th} < P_m < 2\varepsilon_0 \varepsilon_d E_{th}) & (1) \\ E_{c0} + \dfrac{d}{h} E_{th} \qquad (P_m > 2\varepsilon_0 \varepsilon_d E_{th}) & (2) \end{cases}$$

where E_{c0} is the intrinsic coercive electric field in the ferroelectric layer, P_m is the maximal polarization, ε_0 is the permittivity in vacuum, and E_{th} is the threshold field in the dielectric layer. If the electric field in the dielectric passive layer E_d is lower than E_{th}, the passive layer behaves as an insulator, whereas it behaves as a conductor if $E_d > E_{th}$.

We now attempt to explain the experimental data shown in Fig. 3 using Tagantsev and Stolichnov's equations. First, additional data at a low applied electric field were obtained for 8 capacitors containing the films whose P–E characteristics are shown in Fig. 3, and the relationships between P_m and E_c were plotted, as shown in Fig. 6. In this experiment, the applied electric field was varied from 0.45 to 1.1 MV/cm. Since eq. (1) can be rewritten as eq. (3), each set of the data was fitted to a straight line using the least-squares method.

$$E_c = aP_m + b \tag{3}$$

$$a = \frac{d}{\varepsilon_0 \varepsilon_d h} \tag{4}$$

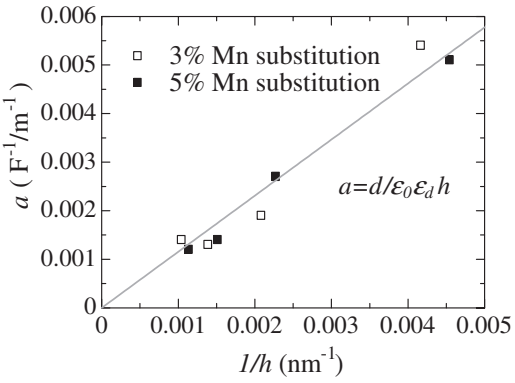

(a)

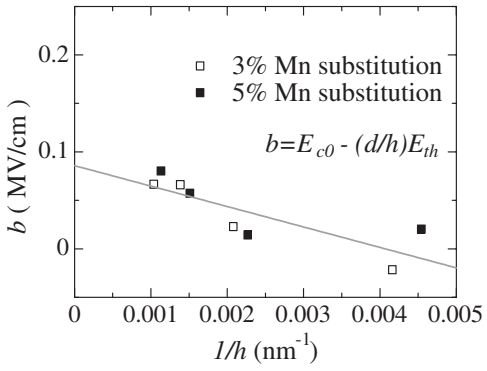

(b)

Fig. 7. Variation of the coefficients a and b with the reciprocal value of film thickness.

$$b = E_{c0} - \frac{d}{h}E_{th} \tag{5}$$

It can be seen from the figures that all the experimental data can be represented using eq. (1) without significant deviation.

In this fitting process, eight pairs of linear regression coefficients, a and b, were obtained. Since the film thickness is nearly equal to h, it is shown from eqs. (4) and (5) that a is inversely proportional to the film thickness and b varies linearly with the reciprocal value of the film thickness. Thus, the coefficients a and b derived from Fig. 6 were plotted against the reciprocal value of the film thickness. The results are shown in Fig. 7, where the horizontal axis is approximately expressed by $1/h$. As can be seen from Fig. 7, the data are somewhat dispersed and it is difficult to distinguish the two sets of data that correspond to the 3 and 5% Mn-substituted films. Thus, the optimal proportionality factor for all data was determined from Fig. 7(a) using the least-squares method, while both the slope and the intercept were determined from Fig. 7(b).

The slope of the line in Fig. 7(a) is proportional to d/ε_d in the dielectric passive layer, and this value can be expressed by the equivalent oxide thickness (EOT), although we cannot determine the individual values of d and ε_d. The average EOT for Mn-substituted BFO films formed on Pt electrodes is 4.5 nm. The decrease of the EOT is important in improving the ferroelectric properties of BFO films, which might be realized by replacing Pt electrodes with $SrRuO_3$ electrodes. Similarly, we can obtain the intrinsic coercive field in the ferroelectric layer from the intercept with the vertical axis in Fig. 7(b). The obtained value is approximately 90 kV/cm. It is interesting to note that the intrinsic coercive field is much lower than the observed values, but still several times higher than the value in a single-crystal BFO film grown by spontaneous crystallization in air from a Bi_2O_3–Fe_2O_3 flux ($E_c = 12$ kV/cm).[12]

5. Conclusions

The film thickness dependences of the polarization characteristics were measured in Mn-substituted $BiFeO_3$ films formed on Pt electrodes by chemical solution deposition. XRD analysis revealed the existence of dielectric passive layers on the Pt electrodes. Excellent P–E hysteresis loops were obtained for the films thicker than 200 nm, but the coercive electric field was relatively high when the film thickness was close to 200 nm. Capacitor models were used to explain the high coercive field and the charge injection model proposed by Tagantsev and Stolichnov was used to fit the experimental data. The conclusions derived from the model fitting are (1) the BFO films have dielectric passive layers and their EOT value is 4.5 nm, and (2) the intrinsic coercive electric field in the ferroelectric layer is approximately 90 kV/cm.

Acknowledgments

This work was performed under the auspices of the Special Coordination Funds for Promoting Science and Technology supported by the Ministry of Education, Culture, Sports, Science, and Technology.

1) J. Wang, J. B. Neaton, H. Zheng, V. Nagarajan, S. B. Ogale, B. Liu, D. Viehland, V. Vaithyanathan, D. G. Schlom, U. V. Waghmare, N. A. Spaldin, K. M. Rabe, M. Wuttig, and R. Ramesh: Science **299** (2003) 1719.
2) S. K. Singh, K. Maruyama, and H. Ishiwara: Appl. Phys. Lett. **88** (2006) 262908.
3) Z. Y. Zhong, S. K. Singh, K. Maruyama, and H. Ishiwara: Jpn. J. Appl. Phys. **47** (2008) 2230.
4) S. K. Singh, N. Menou, H. Funakubo, K. Maruyama, and H. Ishiwara: Appl. Phys. Lett. **90** (2007) 242914.
5) W. J. Merz: J. Appl. Phys. **27** (1956) 938.
6) A. K. Tagantsev and G. Gerra: J. Appl. Phys. **100** (2006) 051607.
7) S. K. Singh and H. Ishiwara: Jpn. J. Appl. Phys. **44** (2005) L734.
8) J. F. M. Cillessen, M. W. J. Prins, and R. M. Wolf: J. Appl. Phys. **81** (1997) 2777.
9) J. J. Lee, C. L. Thio, and S. B. Desu: J. Appl. Phys. **78** (1995) 5073.
10) P. K. Larsen, G. J. M. Dormas, D. J. Taylor, and P. J. van Veldhoven: J. Appl. Phys. **76** (1994) 2405.
11) A. K. Tagantsev and I. A. Stolichnov: Appl. Phys. Lett. **74** (1999) 1326.
12) D. Lebeugle, D. Colson, A. Forget, and M. Viret: Appl. Phys. Lett. **91** (2007) 022907.